Saline tracer visualized with three-dimensional electrical resistivity tomography: Field-scale spatial moment analysis

Kamini Singha and Steven M. Gorelick

Department of Geological and Environmental Sciences, Stanford University, Stanford, California, USA

Received 2 July 2004; revised 18 January 2005; accepted 14 February 2005; published 24 May 2005.

[1] Cross-well electrical resistivity tomography (ERT) was used to monitor the migration of a saline tracer in a two-well pumping-injection experiment conducted at the Massachusetts Military Reservation in Cape Cod, Massachusetts. After injecting 2200 mg/L of sodium chloride for 9 hours, ERT data sets were collected from four wells every 6 hours for 20 days. More than 180,000 resistance measurements were collected during the tracer test. Each ERT data set was inverted to produce a sequence of 3-D snapshot maps that track the plume. In addition to the ERT experiment a pumping test and an infiltration test were conducted to estimate horizontal and vertical hydraulic conductivity values. Using modified moment analysis of the electrical conductivity tomograms, the mass, center of mass, and spatial variance of the imaged tracer plume were estimated. Although the tomograms provide valuable insights into field-scale tracer migration behavior and aquifer heterogeneity, standard tomographic inversion and application of Archie's law to convert electrical conductivities to solute concentration results in underestimation of tracer mass. Such underestimation is attributed to (1) reduced measurement sensitivity to electrical conductivity values with distance from the electrodes and (2) spatial smoothing (regularization) from tomographic inversion. The center of mass estimated from the ERT inversions coincided with that given by migration of the tracer plume using 3-D advective-dispersion simulation. The 3-D plumes seen using ERT exhibit greater apparent dispersion than the simulated plumes and greater temporal spreading than observed in field data of concentration breakthrough at the pumping well.

Citation: Singha, K., and S. M. Gorelick (2005), Saline tracer visualized with three-dimensional electrical resistivity tomography: Field-scale spatial moment analysis, *Water Resour. Res.*, *41*, W05023, doi:10.1029/2004WR003460.

1. Introduction

[2] Over the last 20 years, conducting and interpreting extensively monitored field-scale tracer tests have dramatically improved the understanding of solute transport through heterogeneous media. These field experiments, such as those conducted at Canadian Base Borden, the Massachusetts Military Reservation, and the Columbus Air Force Base have required dense networks of multilevel monitoring wells and intensive sampling [*Freyberg*, 1986; *Mackay et al.*, 1986; *LeBlanc et al.*, 1991; *Boggs et al.*, 1992]. These field experiments are expensive, time-consuming, and generally impractical for most investigations.

[3] Geophysical methods offer cost-effective, spatially exhaustive data. Such data can be used to construct a sequence of snapshot tomograms in 3-D. Often geophysical data have limited utility for analysis of groundwater flow because the properties measured in a geophysical survey are not simply related to the hydraulic properties of interest. However, in the case of monitoring the transport of a conductive tracer using electrical resistivity tomography (ERT) there is a direct physical link between changes in electrical conductivity and changes in ionic solute concentration. ERT readily detects changes in fluid electrical conductivity and the degree of saturation of the porous medium. ERT has been used extensively for monitoring time-varying processes in the vadose zone [*Daily et al.*, 1992; *Park*, 1998; *Binley et al.*, 2002; *Yeh et al.*, 2002] and to map subsurface transport of conductive tracers in 2-D laboratory studies [*Binley et al.*, 1996; *Slater et al.*, 2000], 2-D field studies [*Kemna et al.*, 2002; *Acworth and Dasey*, 2003], and a 3-D laboratory study [*Slater et al.*, 2002].

[4] Despite these and other case studies, analysis and interpretation of ERT images remain challenging for two reasons. First, geophysical tomographic inverse problems are typically underdetermined; there are not enough data to uniquely estimate the values of the geophysical model parameter values. Second, ERT inversion is a highly nonlinear problem, so a small change in the data can cause a large change in the solution; the inverse solutions are sensitive to error and noise in the data. Because the ERT inversion in this work has been defined as an underdetermined problem, the tomogram is stabilized through a process of regularization. Regularization procedures work by imposing additional constraints to achieve a more simple solution, where simplicity is usually described by the smoothness or uniformity of the image [e.g., *Beck et al.*, 1985]. Regularization for our ERT inverse problem can be thought of simply as the math-

0043-1397/05/2004WR003460$09.00

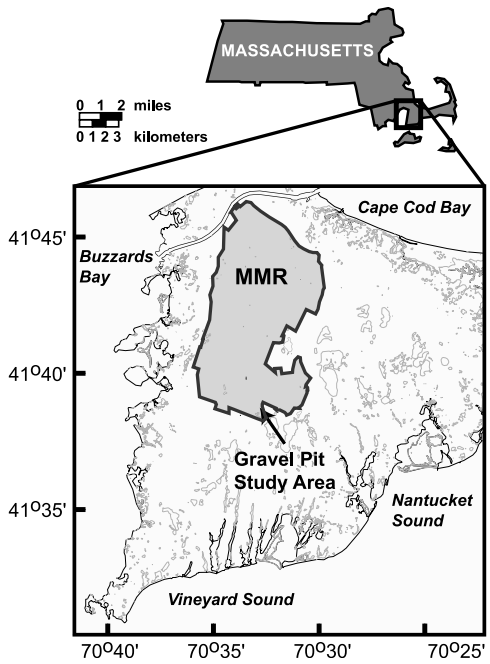

Figure 1. Location of field site at the Massachusetts Military Reservation, Cape Cod, Massachusetts, at which the combined cross-well ERT and sodium chloride tracer experiment were conducted.

ematical process undertaken during tomographic inversion that determines the additional information needed to obtain the smoothest model that explains the data.

[5] As a consequence of the above difficulties, over-parameterized tomographic images are smoothed and their accuracy varies spatially. The ability of the geophysical method (ERT) to measure the geophysical parameter of interest (electrical conductivity) is limited by regularization, the survey geometry, and the physics underlying the measurements. Spatially variable resolution leads to heterogeneity in the reliability of the image. To study and partially overcome some of the above difficulties, *Day-Lewis and Lane* [2004] and *Singha and Moysey* [2004] used 2-D hypothetical examples to illustrate how the correlation between the measured geophysical parameter and the hydrogeologic property of interest varies spatially. This correlation between the geophysical parameter (e.g., dielectric permittivity) and the aquifer property (e.g., water content) can be quantified through the model resolution matrices or through assessment of ensemble statistics taken from multiple dielectric permittivity realizations analyzed for water content. These two prior studies, aimed at quantifying resolution, were computationally feasible in 2-D. Unfortunately, it is difficult to manipulate 3-D resolution matrices, which for our work are of approximate dimension 150,000 by 150,000, to quantify 3-D variability in spatial resolution.

[6] Here we present two contributions. First and foremost we show the results from an original hydrogeophysical field experiment in which ERT data were collected during a month-long forced-gradient sodium chloride (NaCl) tracer test. The geophysical data reflect changes in electrical conductivity caused by changes in groundwater salinity from transport of ionic tracer. Second, we present snapshot tomograms showing the movement of the tracer, and results from modified moment analysis applied to the electrical conductivity (the reciprocal of resistivity) tomograms to quantify the tracer mass, center of mass, and spatial variance. On the basis of this analysis we demonstrate how (1) the center of mass is accurately mapped when ERT is sufficiently sensitive to the presence of the ionic tracer and (2) the spatial variability in resolution causes significant yet predictable underestimates of tracer mass.

2. Site Description

[7] Our field research was conducted at the U. S. Geological Survey Toxic Substances Hydrology Program research site at the Massachusetts Military Reservation (MMR) in western Cape Cod, Massachusetts (Figure 1). The site is composed of unconsolidated glacial and outwash plain deposits, consisting primarily of stratified sand and gravel [*Oldale*, 1969]. At the site, the glacial outwash is approximately 35 m deep, generally fining with depth. The outwash is underlain by finer, less permeable, proglacial lake deposits consisting of sand, silt, and clay [*Garabedian and LeBlanc*, 1989; *Masterson et al.*, 1997]. The water table was 5.5 m below ground surface. Groundwater flows predominantly through the shallow, coarser-grained parts of the aquifer. The estimated mean horizontal hydraulic conductivity ranges from 85 to 115 meters per day (m/d) in the medium to coarse sands and gravels, and varies by approximately an order of magnitude [*LeBlanc et al.*, 1991; *Masterson et al.*, 1997]. The ratio of horizontal to vertical hydraulic conductivity has been estimated to be on the order of 2:1 to 5:1 as characterized by numerous field-scale aquifer tests [*Masterson et al.*, 1997], and the average groundwater velocity is 0.2–0.7 m/d [*LeBlanc*, 1984]. A prior estimate of effective porosity was 0.39 [*LeBlanc et al.*, 1991] for the greater MMR region, and we found a value of 0.28 based on analysis of solute breakthrough at our experimental site. An irregular bedrock surface, beneath approximately 100 m of unconsolidated materials, is much less permeable than the overlying glacial deposits, and therefore serves as the bottom of the regional groundwater system [*Garabedian and LeBlanc*, 1989; *Masterson and Barlow*, 1994].

[8] Our field experiment was conducted in the F626 borehole array in the "gravel pit study area" (Figure 1) at the southern end of the MMR. The gravel pit study area is downgradient from a sewage treatment facility that discharged secondarily treated effluent from 1936–1995 [*LeBlanc et al.*, 1999]. Consequently, the pore fluids on site had total dissolved solids that exceeded the concentration of the native groundwater [*LeBlanc et al.*, 1991]. The F626 array used for this tracer test consists of six polyvinylchloride (PVC) wells and a multilevel sampler. The area contained within the F626 array is approximately 10 $\times$ 14 m in plan view. The wells are aligned in two perpendicular planes (Figure 2). The four ERT wells (F626A-D) are 33.0 m deep and fully screened, which allow the ERT electrodes to be in electrical contact with the formation. The fully screened injection and pumping

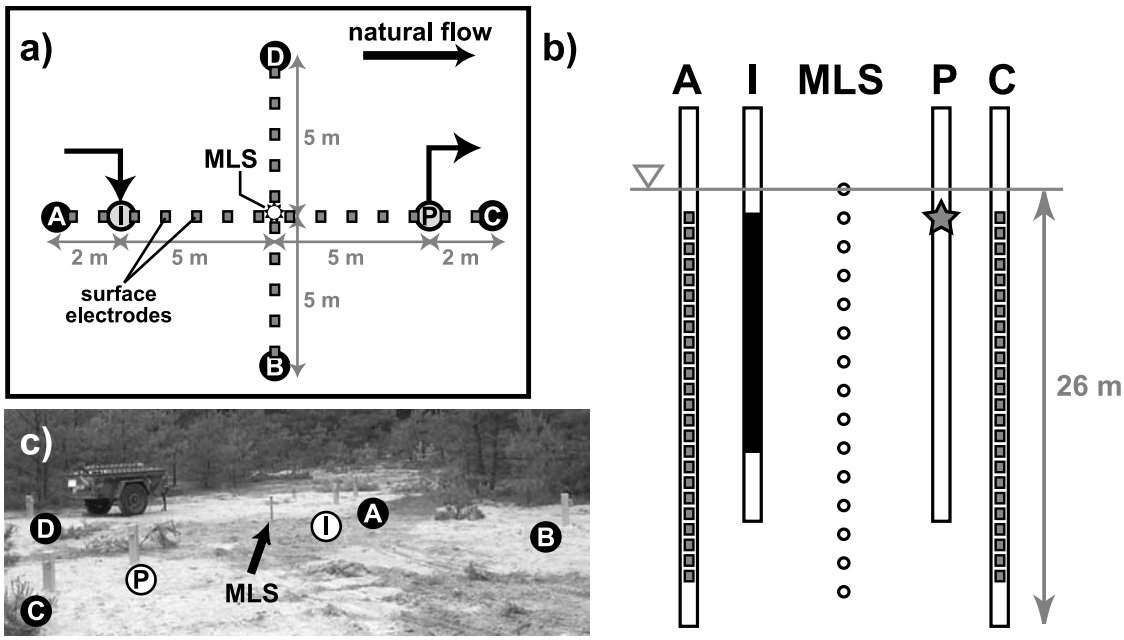

Figure 2. Geometry of experimental well field in (a) map view and (b) side view parallel to transport as well as in (c) a photograph of the site (not aligned to schematics). ERT wells are labeled A-D. Injection and pumping wells are labeled I and P, respectively. MLS is the multilevel sampler. The distance between ERT wells A and C is 14 m, and the distance between the ERT wells B and D is 10 m, as shown in Figure 2a. The injection line, shown in well I as a solid black line in Figure 2b, extends from 7 to 22 m. The MLS ports are shown as open circles in Figure 2b and are separated by 1.8 m (6 feet). The water table is at approximately 5.5 m. The ERT electrodes are 1 m apart from 7 to 30 m below ground surface. The outtake for the pump in the fully screened pumping well is marked by a star in Figure 2b and is at approximately 7 m below ground surface. Surface electrodes, used for synthetic ERT modeling, are separated by 1 m horizontally and are shown in Figure 2a.

wells, F626I and F626P, are 26.5 m deep and separated by a distance of 10 m.

3. Methods

3.1. Electrical Resistivity Tomography Forward Problem

[9] Cross-well ERT is used to estimate the distribution of electrical conductivity in the subsurface from numerous resistance data calculated by establishing an electrical gradient between two source electrodes and measuring the resultant potential distribution at two or more receiver electrodes. The measured resistances are averages of the electrical properties of the rock and conductive fluid in the system [*Keller and Frischknecht*, 1966]. For this study, this procedure was repeated for 3150 combinations of source and receiver electrode positions.

[10] The governing Poisson equation describes the electrical potential distribution as:

$$-\nabla \cdot \sigma \nabla \phi = I\delta\left(x_1 - x_{1,s}, x_2 - x_{2,s}, x_3 - x_{3,s}\right) \tag{1a}$$

subject, in this work, to Neumann boundary conditions $\left(\frac{\partial \phi}{\partial n_i}\right) = 0$, where

ϕ the electrical potential in volts (V);
σ the electrical conductivity in Siemens/m (S/m);
I the electrical current source in amperes (A);
δ the Dirac delta function;
x_1, x_2, x_3 the 3-D Cartesian coordinates;
$x_{i,s}$ the coordinates of the point source of injected charge (m);
n_i the direction normal to each boundary i.

In this study, the model boundaries are approximately 130 m from the well locations in map view and extend a similar distance beneath the bottom ERT electrode. The finite element mesh extends significantly beyond the region of interest so that the effect of the boundary conditions is minimal.

[11] Resistance is the dependent variable matched during tomographic inversion to estimate the 3-D electrical conductivity field. On the basis of the solution to (1a) each resistance value can be calculated using Ohm's law, given here for a point source:

$$R = \frac{\Delta \phi}{I} \tag{1b}$$

where R is the resistance in ohms.

[12] Because current flows spherically from each point source, an important physical property is that current density decreases away from the electrodes. It is therefore intuitive that measurement sensitivity would likely be highest near the electrodes.

[13] In our experiment, which consists of injecting tracer under a forced hydraulic gradient, the measured resistances are averages of the aquifer material and the solute. The electrical resistance of the bulk media changes as the tracer migrates from the pumping to the injection well. The local

electrical conductivities vary with time reflecting the extent and local concentrations of the tracer plume.

3.2. Electrical Resistivity Tomography Inverse Problem

[14] Given cross-well resistance data collected in the field, the goal is to invert the ERT data to construct the 3-D spatial distribution of the subsurface electrical conductivity. Calculating the true distribution of electrical conductivity in the subsurface is a highly nonlinear problem because the current paths through the medium are dependent on the electrical conductivity structure. Because of the nonlinear relationship the ERT inverse problem is solved using iterative inversion [*Tripp et al.*, 1984; *Daily and Owen*, 1991; *LaBrecque et al.*, 1996]. Although the geophysical inverse problem is not always underdetermined [e.g., *Lane et al.*, 2004], other data about the distribution of system characteristics are required to create a model with fewer parameters. Generally, as in our case, the tomographic inverse problem is overparameterized; there are generally more model parameters to be solved for than independent measured field data. For this work, each snapshot is composed of nearly 150,000 electrical conductivity unknowns, with approximately 33,000 unknowns in the area of interest and the rest as boundary elements. These electrical conductivity values are estimated based on 3150 resistance measurements.

[15] In ERT data collection a finite number of imprecise resistance measurements are collected, which often do not provide enough information to uniquely determine all the local electrical conductivity parameter values. As discussed previously, the tomographic inverse problem is consequently underdetermined and ill posed and has no unique solution. Ill-posed inverse problems require additional information for an acceptable solution to be found. It can be difficult to collect the necessary data to make the problem well-posed in field experiments where heterogeneity is complicated and data are limited [*McLaughlin and Townley*, 1996]. In addition, data errors create ill conditioning. To determine a solution consisting of discrete electrical conductivity values, we regularize the inverse problem, which in this work smoothes the final electrical conductivity field thereby inducing correlation and effectively reducing the number of unique local values that must be independently estimated. Other approaches to obtain a unique solution to the ERT inverse problem are also possible and might result in less smoothing [*Yeh and Simunek*, 2002].

[16] The solution to the inverse problem is a 3-D map of electrical conductivity values and is based on nonlinear least squares minimization of a two-part objective function. The first part is the misfit between the predicted and measured resistance values. This part of the objective minimizes the discrepancy between ERT data and the computed resistances based on (1a) and (1b). The second part is the regularization term. It minimizes the roughness of the electrical conductivity field and allows for well posedness of the inverse problem. For ERT inversion this objective function is given by

$$\Omega = \| Wd - WG(m) \|^2 + \alpha \| D^T Dm \|^2 \qquad (2)$$

where

- W a diagonal matrix used to weight individual resistances;
- d the measured data (resistances) obtained in the field from tomography;
- m the estimated parameter values (log electrical conductivity, σ), used in the electrical flow model (1a);
- $G(m)$ the resistances calculated from the forward solution of (1a) and (1b) given log electrical conductivity values m;
- α the regularization parameter that determines the importance given to the smooth appearance of the electrical conductivity field relative to the misfit between calculated and observed resistances;
- D a roughness matrix, which in this study, is based on a discretized second derivative operator for the six immediate neighbors to each voxel.

A small α will minimize the residual error between measured and modeled resistances but may not converge to a unique solution, whereas a large α will identify an overly smooth electrical conductivity field that may not fit the measured field data (resistances) well [see, e.g., *Tikhonov and Arsenin*, 1977], D can also be the covariance of the model parameters, which in this case are the electrical conductivities values [*Tarantola*, 1987; *Gouveia and Scales*, 1997; *Kitanidis*, 1997; *Vasco et al.*, 1997; *Day-Lewis et al.*, 2003]. The ERT inversion routine used for this work is based on Occam's approach [*Constable et al.*, 1987; *de Groot-Hedlin and Constable*, 1990; *LaBrecque et al.*, 1996] and written by Andrew Binley of Lancaster University. The regularization is controlled by the roughness matrix D and the regularization parameter α. The effect of regularization is to smooth the electrical conductivity distribution and stabilize the inverse solution. The regularization scheme penalizes the electrical conductivity model's roughness, imposing an a priori preference for a smooth final model. With regularization, the final electrical conductivity parameters will not have extremely small or large values unless they are essential to match the data [*Constable et al.*, 1987; *Sasaki*, 1989; *Ory and Pratt*, 1995]. The regularization parameter, α, controls the degree of smoothing of the estimated conductivity field. Ideally, the value of α is selected such that the match to the field data is consistent with the estimate of expected measurement errors. Here, we use an approach in which a target root-mean-square (RMS) error is defined based on reciprocal measurements, which are described by *Binley et al.* [1995]. At each iteration of the inversion, a line search is performed to identify the α value that results in the lowest RMS error not exceeding the target RMS error [*LaBrecque et al.*, 1996]. The optimal estimated electrical conductivity field is the one which explains the measured resistances to an acceptable degree (i.e., yields the target root-mean-square error) and minimizes the roughness of the estimated conductivity field. The bicriteria objective allows the magnitude of the smoothing of simulated electrical conductivity values to vary spatially; smoothing can be larger in areas of the tomogram with low data sensitivity. In regions with higher sensitivities, estimated local values are expected to be more precisely determined with less smoothing. The final result of the ERT inversion is a smooth 3-D map of electrical conductivity that best

fits the data to a given criteria, and may be more detailed in areas of high sensitivity and smooth in areas of low sensitivity.

[17] For each iteration, the system is linearized and a Gauss-Newton update of the form $m_i + \Delta m \rightarrow m_{i+1}$ is carried out. The parameter change Δm is obtained by solving the linearized system

$$\left(J^T W^T W J + \alpha D^T D\right)\Delta m = J^T W^T W(d - G(m)) - \alpha D^T D m \quad (3)$$

where J is the Jacobian matrix defined as $J = \frac{\partial G(m)}{\partial m}$. At each iteration, the objective function is reevaluated, and the Gauss-Newton process is repeated until the objective function converges to the desired data fit. With a 2.8 GHz Xeon Dell 2650 cluster with 2 GB of RAM, each inversion took approximately 60 hours on a single node.

[18] ERT inversion results are strongly dependent on the error level to which the data are fitted. The conductivity contrasts in the inverted model and the occurrence of artifacts will be dependent on how well the data are fitted. Quantifying the ''correct'' data errors is a crucial issue to using ERT data quantitatively. The target data error level for inversions performed here was based on the observed discrepancy between normal and reciprocal measurements from the field data (maximum value is 5%). For this work, we define our misfit tolerance, ε, according to error variance model parameters a and b where

$$\varepsilon = a + b|R| \quad (4)$$

as defined by *Slater et al.* [2000]. For the field inversions, we used $a = 0.01$ ohms and $b = 0.05$.

3.3. Relation Between Electrical Conductivity and Solute Concentration

[19] Of interest in our time lapse analysis is the temporal change in ERT-estimated NaCl concentration, ΔC. We estimate changes in NaCl concentration from changes in bulk electrical conductivity using Archie's law [*Archie*, 1942] in combination with a linear regression constructed from fluid samples collected at the multilevel sampler that reflects the linear relation between fluid electrical conductivity in mS/m and chloride concentration in mg/L at the sample scale,

$$\Delta C_{Cl-} = 3.19 \cdot \Delta\sigma_f \quad (5)$$

where $\Delta\sigma_f$ is the change in fluid electrical conductivity from the background as measured using a handheld Orion specific conductance meter. The linear regression had an $R^2 = 0.98$. The estimated chloride concentration was used to calculate the NaCl concentration of the fluid samples. Temperature effects are negligible and are not considered in this study.

[20] The presence of solid media also affects the relation between electrical conductivity and solute concentration. We used Archie's law, based on changes, in which

$$\Delta\sigma_f = F \cdot \Delta\sigma_b \quad (6)$$

where $\Delta\sigma_b$ is the change in bulk electrical conductivity from the background in mS/m, and F is the unitless formation factor. The formation factor has been defined in the literature in various ways [*Wyllie and Rose*, 1950; *Archie*, 1952; *Winsauer et al.*, 1952] but was originally defined as

$$F = n^{-\zeta} \quad (7)$$

in which n is the effective porosity and ζ is the cementation exponent, which is related to connectedness of pore space [*Guyod*, 1944] and is generally less than 2 for poorly cemented materials [*Keller and Frischknecht*, 1966]. Colocated measurements of fluid and bulk ERT electrical conductivity and the multilevel sampler location in the field gives a formation factor of 5, which would indicate a value of ζ from 1.3 to 1.7 depending on the effective porosity, which is $\sim$0.28 based on analysis of solute breakthrough at the pumping well. Because there are no extensive data for effective porosity at our 10 m by 14 m experimental site, we use the mean value estimated tracer breakthrough. As commonly practiced, spatial variations were necessarily neglected. If the formation factor, used in (7), varies in space associated with changes in effective porosity or cementation exponent, the relative change in local bulk electrical conductivity can still be interpreted as an absolute change in concentration provided that surface conduction can be neglected and the background fluid electrical conductivity is relatively constant [*Kemna et al.*, 2002]. However, an incorrect estimate of the effective porosity will of course affect the estimated mass value.

3.4. Moment Analysis

[21] For this analysis, 3-D spatial moments were calculated from the ERT tomograms according to

$$M_{ijk}(t) = n \int\int\int_{\Gamma} \Delta C(x,y,z,t) x^i y^j z^k dx dy dz \quad (8)$$

where

M_{ijk}	the spatial moment of interest;
i,j,k	exponents with values 0 to 2, whose value(s) depend on the particular moment of interest;
n	the effective porosity, assumed constant;
ΔC	the ERT-estimated change in concentration, where the background bulk electrical conductivity has been removed;
x,y,z	Cartesian coordinates;
dx,dy,dz	the voxel dimensions in the x, y, and z directions;
Γ	the test domain within the volume of interest.

The zeroth moment, M_{000}, is the mass in the system. The first moment (M_{100}, M_{010}, M_{001}) normalized by the mass, defines the center of mass of the tracer in each principal direction. The variance or covariance of the tracer plume is related to the second spatial moment (8) (M_{200}, M_{020}, M_{002}, M_{110}, M_{101}, M_{011}), center of mass, and tracer mass. For example, in the direction of transport,

$$\sigma_X^2 = \frac{M_{200}}{M_0} - \left(\frac{M_{100}}{M_0}\right)^2 \quad (9)$$

Table 1. Input Parameters for Flow and Transport Model

Parameter	Value
Hydraulic conductivity	K_H = 100 m/d, K_V = 50 m/d
Porosity	0.28
Natural gradient prepumping	0.001
Dispersivities	α_{11} = 0.6 m, α_{22} = 0.06 m, α_{33} = 0.006 m
Molecular diffusion coefficient	3×10^{-6} of m^2/d
Injection rate	13.3 L/min
Pumping rate	38.6 L/min
Background concentration	65 mg/L
Fresh water concentration	12 mg/L
Tracer concentration	2200 mg/L

whereas the spatial covariance in the X-Y plane is defined as

$$\sigma_{XY}^2 = \frac{M_{110}}{M_0} - \left(\frac{M_{100} \cdot M_{010}}{M_0^2}\right) \tag{10}$$

as highlighted by *Liu et al.* [2004]. Estimates of the dispersion coefficient, D, are related to the second spatial moment [*Aris*, 1956], such that

$$D = \frac{1}{2}\frac{\partial \sigma^2}{\partial t}. \tag{11}$$

4. Solute Transport and Electrical Flow Simulations

[22] Prior to conducting the field experiment, we used numerical simulation to calculate the spatial moments we expect to see in the field using ERT. Two types of simulation models were employed. First is advective-dispersive transport simulation to represent expected plume behavior. Second is electrical flow modeling and tomographic inversion, which mimics the ERT data collection and imaging process. The numerical simulations were created considering the realities of expensive fieldwork and data collection; in practice there are budgetary and logistical limitations in field surveys that limit the number of wells. Needing few monitoring wells is one of the presumed virtues of cross-well tomography. Consequently, we create synthetics using 4 ERT wells and surface electrodes. Additionally, continuous automated ERT data collection was limited to 6300 total data points, reciprocals included, for each snapshot of the plume. There were 60 ERT snap shots in all. Collecting more data to detect the migrating plume would have resulted in additional temporal smearing when the snapshot was analyzed.

[23] By simulating a tracer plume and then creating synthetic resistance data sets, hypothetical yet realistic tomograms were produced that should mimic the expected field results. We then took each tomogram and predicted the spatial moments of the idealized electrical conductivity field. These moments were then compared to the moments computed for the simulated tracer concentrations. The benefit of this synthetic tracer test is that it is completely controlled, yet the resulting ERT inversions of snapshots of these synthetics should mimic the field conditions well enough to provide insight into the field experiment.

4.1. Hydrogeophysical Simulation Approach

[24] The average behavior of the tracer transport for this field-scale tracer test and its affect on the geophysical signal were modeled through a five-step process of (1) steady state flow modeling using MODFLOW-96 [*Harbaugh and McDonald*, 1996], (2) tracer transport modeling with MT3DMS [*Zheng*, 1990; *Zheng and Wang*, 1999], (3) conversion of tracer concentration to bulk electrical conductivity following Archie's law (6), (4) forward modeling of ERT based on (1), and (5) subsequent inverse modeling of the forward model resistances based on (2).

[25] The flow and transport model was based on the average properties at the MMR field site including an anisotropic homogeneous hydraulic conductivity. The details of the parameter values, conditions, and rates used in the models are listed in Table 1. Two constant head boundaries are implemented in the flow model 130 m respectively from the injection and pumping wells to produce the natural gradient of 0.001 measured in the field. The two boundaries perpendicular to transport are represented as no flow conditions, also a distant 130 m from the area of interest. The location of the transport model boundaries coincide with the flow model boundaries, and are constant concentration boundaries set at the mean NaCl background concentration of 65 mg/L.

[26] The tracer was injected over a depth interval extending from 7.0 to 22.2 m below ground surface in the injection well. An injection rate of 13.3 L/min and a pumping rate of 38.6 L/min were used for the entire duration of the test. The injection rate was varied with depth; the injection rate was higher near the top of the well than at depth as quantified from fluid conductivity measurements and electromagnetic induction logs in the injection well. The injection regime included 8 days of freshwater injection, with a concentration of 12 mg/L, followed by 9 hours of a conservative tracer, with a concentration of 2200 mg/L, and 20 days of freshwater. Without exact information on field porosities and expected dispersivities for this doublet tracer test, we ran numerous transport simulations with various porosities and dispersivities, and show in this work the simulation that best matched the concentration history measured in the pumping well during the field experiment. For the simulations shown here, the effective porosity was 0.28. The dispersivities that match the field data were approximately 1/2 the dispersivities observed by *LeBlanc et al.* [1991] and *Garabedian et al.* [1991] for a nearby natural-gradient tracer test. This is expected given that the natural gradient test has a transport scale of approximately 280 m, which is 28 times the well-to-well scale in this study, so our tracer test is indicative of a local-scale dispersivity value while the latter reflects a macrodispersivity for the entire field. Weak-doublet tracer tests have much lower dispersivities than those seen in natural gradient tests, especially when considering small well separations with respect to the heterogeneity [*Tiedeman and Hsieh*, 2004]. The estimated correlation length of ln (hydraulic conductivity) is 5 m [*Hess et al.*, 1991] which is about one half of our interwell distance. As shown in Figure 3, the concentration history at the simulated pumping well closely matches the field data. From solute transport simulation, the maximum NaCl concentration at the pumping well is approximately 85 mg/L, which matches that measured in the field.

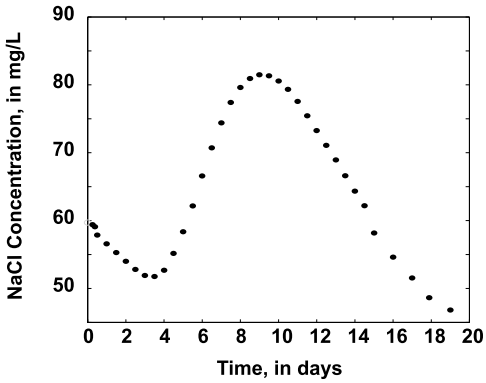

Figure 3. Concentration history at pumping well based on 3-D advective-dispersive transport simulation. Day zero corresponds to the start of the tracer test. The tracer was injected at the injection well beginning at time zero and continued for 9 hours. The elapsed time to peak arrival at the pumping well from the start of the injection period was approximately 9 days.

[27] Results at forty different times from the transport simulation model, ranging from pretracer injection to 23 days postinjection, were converted to fluid electrical conductivities through the linear relation based on regression calculated from the field samples (5). The tracer concentrations were converted to fluid electrical conductivities using the linear regression based on fluid samples from the multilevel sampler and then to bulk electrical conductivities through Archie's law (6), disregarding matrix conduction and assuming a formation factor of 5.

[28] The geometry of the 4 ERT wells in the synthetic models followed the configuration planned for the field experiment (Figure 2), with 24 electrodes per well, with 1-m separation between electrodes located at 7.0 to 30.0 m below ground surface. Using the same nodal mesh for inversion of the field data, the Poisson equation (1) was solved to obtain 3150 forward model resistances between four ERT wells. Adding no noise, the simulated resistances were treated as "observations" and were inverted to obtain the ERT-estimated electrical conductivities according to (3) with a homogeneous starting model, initially constant observation weights, a discretized second-derivative roughness filter, and error misfit criteria based on the average forward modeling errors. Solute mass based on the ERT inversions was calculated between snapshots using (8). Moments were calculated from the ERT inversions with and without surface electrodes.

[29] An additional synthetic case was also run that was identical to that described above but also contained a surface resistivity array. Twenty-four surface electrodes were placed 1 m apart in two perpendicular lines between the ERT wells as shown in Figure 2, and 3200 forward model resistances were inverted to obtain maps of electrical conductivity through time.

4.2. Moments Estimated From Synthetic ERT Experiments

4.2.1. Zeroth Moment

[30] The injected mass in the transport model, calculated using (8) after removing the mass from the background concentration, is 15.2 kg (Figure 4a). However, the total change in mass from the maximum to the minimum value is 20.4 kg, indicating that the tracer mass plus higher ambient concentration pore fluid were removed and replaced with lower concentration freshwater. The ERT estimated mass from the synthetic geophysical model without the surface electrodes shows a maximum injected mass of approximately 8.9 kg, or 59% of the actual mass injected into the system, and a change in the maximum-to-minimum concentration of 14.6 kg, or 72% of the total change (Figure 4b). This addition of a surface array does not materially change the mass estimates, improvements in mass associated with the surface array are on the order of 1%, as the water table is approximately 5.5 m below ground surface, and no surface-to-borehole measurements were collected due to expected time limitations on data collection.

[31] Analysis of the ERT-estimated mass from the synthetic cases leads to two conclusions. First, mass estimates from the ERT show especially poor recovery at very early time when the tracer plume is near the injection well. Although there is generally better target recovery near the electrodes and a highly electrically conductive target should serve to channel current and increase the sensitivity in that area, least squares inversion with a discretized second-derivative model filter will produce a smooth final image. The magnitude of the electrical conductivity contrast between the background and the target plume may be affecting the mass recovery. Because the tracer plume is a small target with sharp boundaries, it is difficult for the inversion to recover accurately. The contrast in the electrical conductivities in the transport models at early time varies from approximately 50 mS/m at the center of the plume to 2.4 mS/m at the background. Additional synthetic ERT experiments using simplified cylindrical shapes of varying contrast confirmed that smoothly varying targets, or ones

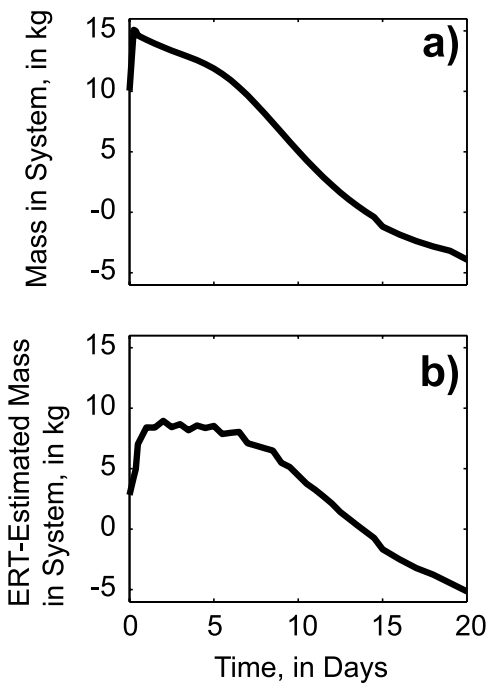

Figure 4. (a) Mass in system based on advective-dispersive transport simulation. (b) Cumulative difference of ERT mass estimated from 3-D synthetic tomograms.

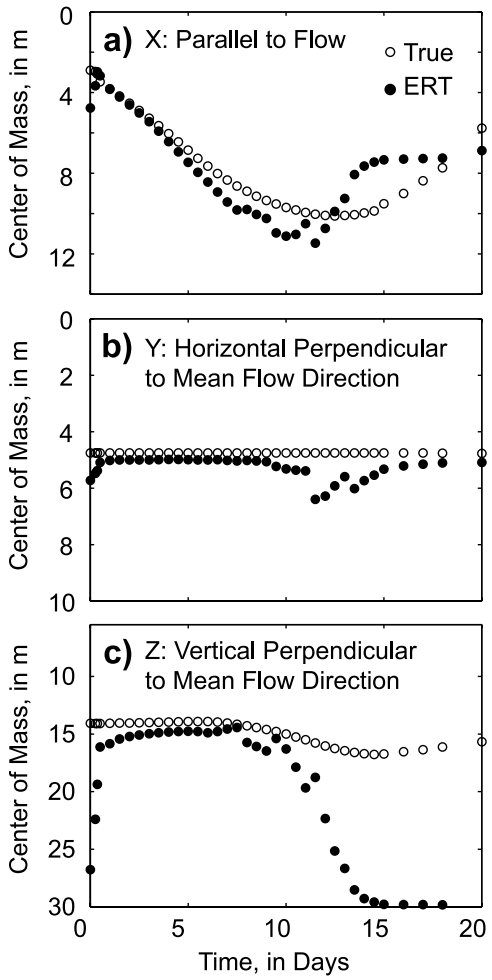

Figure 5. Center of mass calculated from analysis of the synthetic ERT inversions in (a) direction of flow, (b) horizontal perpendicular to the mean flow, and (c) vertical perpendicular to the mean flow direction.

with gradational contrasts, will be better represented than targets with sharp boundaries when using a second derivative regularization filter. Second, in these synthetic examples, there is better mass recovery at later times during the tracer test, once the tracer has advected and dispersed away from the injection well. These results suggest that a low electrical conductivity contrast, if detectable, does not necessarily result in poorer ERT mass recovery than when a higher contrast exists.

4.2.2. First Moment

[32] To accurately estimate the center of mass, the background concentration, 65 mg/L, was removed from the simulated aquifer and from the synthetic tomograms. The center of mass along the flow direction estimated by the ERT is compared to the center of mass of the tracer from transport simulation (Figure 5a). Results show that ERT-estimated velocity of the tracer matches the velocity from transport simulation with and without the presence of surface electrodes. At late times, the center of mass as estimated by the ERT is slightly ahead of the center of mass of the solute plume. This effect may be a function of regularization, which smoothes the resultant inversion around the detected target, and consequently may misrepresent the true location of the center of mass. By day 11, enough mass has been removed from the system by the pumping well that it is not detectable with the synthetic ERT inversions. In the transverse direction, the ERT accurately maps the center of mass along the center line at y = 5 m (Figure 5b) until day 11. The center of mass in the vertical direction remains constant around 16 m when only cross-well data are used, which is slightly below the center of mass of 14 m (Figure 5c) based on tracer transport simulation.

4.2.3. Second Moment

[33] The spatial variance was determined by removing the background concentration from each ERT snapshot and then applying (8). The spatial variances estimated from ERT in this case are unreliable after day 11, when most of the mass has been removed from the system. In the x direction, parallel to transport, there is an increase in the ERT-estimated spatial variance through time parallel to flow between days 0 and 5 when no surface electrodes are used, which may reflect dispersive plume behavior (Figure 6a). The spatial variance increases over time in the direction of transport until the tracer plume is in the center of the ERT array around day 5, and subsequently decreases as the tracer moves toward the pumping well. This increase and decrease in spatial variance is greatly subdued when surface electrodes are used, as this change is likely a function of spatially variable sensitivity; in areas where the data sensitivity is low and the ERT image is smoother, the apparent spatial variance increases. For example, as the tracer is transported closed to the pumping well and the ERT well beyond it, the apparent spatial variance again decreases. From Figure 6 and equation (11), it is clear that estimates of the dispersion coefficient from cross-well ERT alone are too high at early time, and negative at later time as the ERT-estimated tracer plume refocuses near the pumping well as a function of increased resolution.

[34] The ERT-estimated spatial variance remains constant through time in the Y and Z directions, perpendicular to transport (Figures 6b and 6c), likely as a function of reasonably consistent smoothing from regularization in these directions despite the fact that the transport simulations show increasing dispersivity values through time in these directions. The cross-covariance terms in X-Y and Y-Z are nearly zero in the transport simulations, and isotropic regularization does not impose a cross covariance in these directions for the ERT (Figures 6d and 6e). However, there is a small negative, cross-covariance value in X-Z, the plane parallel to transport, in the transport simulations. This is likely due to the variation in injection and pumping rates with depth (Figure 6f). The ERT does a reasonable job of detecting this proper tilt in the plume shape from day 5–10; prior to this time, the ERT cross covariance reflects a tilt in the plume opposite in direction to that observed in the transport simulation.

[35] The spatial variance estimated by the ERT does not replicate exactly that seen in the transport model. This result is not unexpected, given that the ERT data were inverted using a discretized second-derivative model filter, which greatly smoothes the resultant inversions, and spreads the plume location more widely over the area of interest. Using the full covariance matrix, three-dimensional ellipsoids comparing the evolution of the plume from the transport

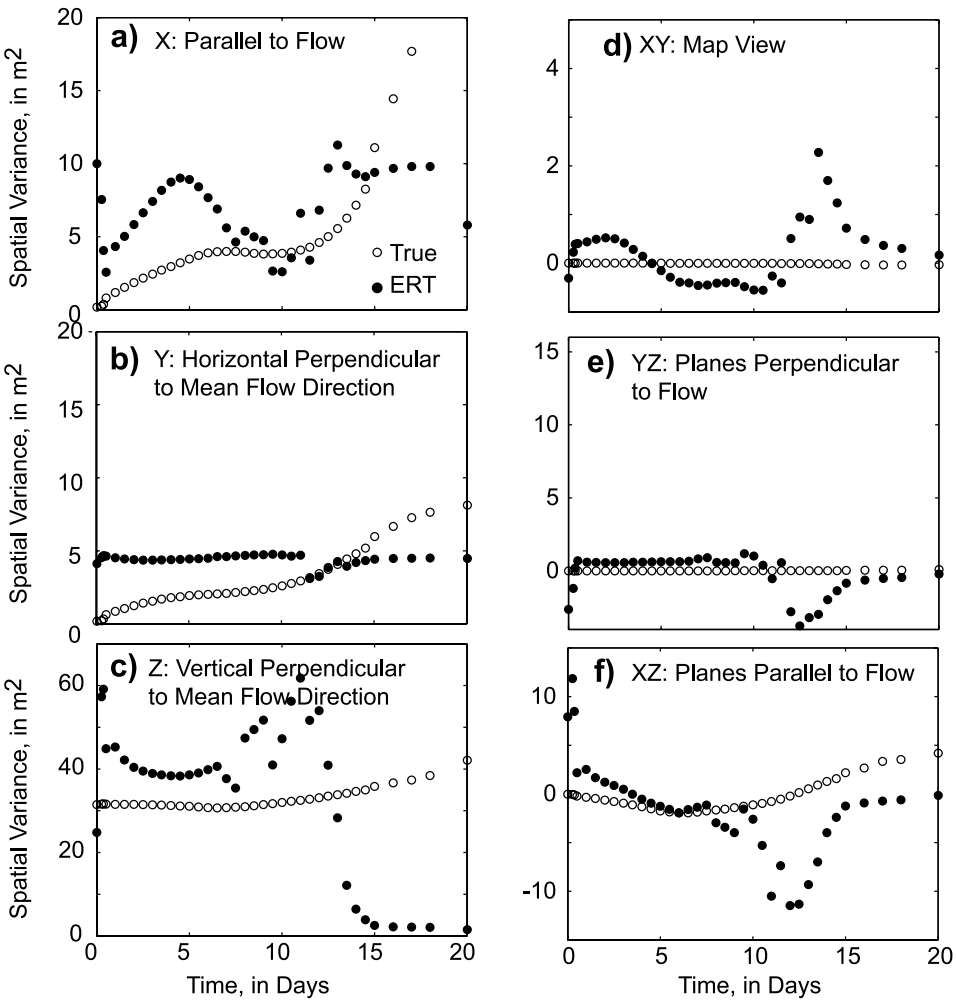

Figure 6. Spatial covariances calculated from analysis of the transport simulations and synthetic ERT inversions in the (a) x direction, parallel to flow, (b) y direction, horizontal perpendicular to the mean flow, and (c) z direction, vertical perpendicular to the mean flow direction and the (d) x-y cross covariance, map view, (e) y-z cross covariance, perpendicular to flow, and (f) x-z cross covariance, parallel to flow.

simulation to those estimated by the ERT were created (Figure 7). The ERT ellipsoids clearly show the overestimation in spatial variance by the ERT, and the change in tilt of the ERT-based plume through time associated with the X-Z cross covariance.

5. Field Experiment

[36] Given the results from the simulations, we conducted a field experiment to estimate spatial moments of a nonreactive tracer in a sand and gravel aquifer. ERT was used to track the transport of the NaCl tracer within the region defined by four corner-point wells (F626A-D). In the field, the use of surface measurements was precluded by very high contact resistances, which did not allow us to drive current into the ground. We conducted a weak-doublet tracer test, in which fluid was continuously pumped at 38.6 liters per minute (L/min) from F626P while injecting continuously at 13.3 L/min from F626I. The tracer was injected over a depth interval extending from 7.0 to 22.2 m below ground surface at well F626I. A permeable tube was inserted into the injection well to evenly distribute the tracer. A weak doublet regime was chosen to ensure maximum capture of the tracer by the pumping well F626P. The pumping well was screened from 5.2 to 26.2 m below the ground surface (Figure 2).

[37] Pumping and injection were carried out for an initial 8-day period to achieve a steady state flow regime. First, low electrical conductivity fresh water (σ_f = 2.4 mS/m, or 12 mg/L NaCl) was injected into the aquifer for 8 days. Once turned on, the pumping and injection wells continued to run for the duration of the experiment. After 8 days, a 2200 mg/L NaCl tracer (σ_f = 470 mS/m) was introduced at F626I for 9 hours. A total of 15.3 kg of NaCl were injected into the aquifer. Although the tracer solution was more dense than the native pore fluid (σ_f = 15 mS/m), density effects should be small because the high injection and even higher pumping rates forced flow to be horizontal, and because tracer dilution readily occurred after injection. We estimate horizontal groundwater flow velocity directly between the two wells to be 1.9 m/d under the forced gradient versus approximately 0.4 m/d under the natural

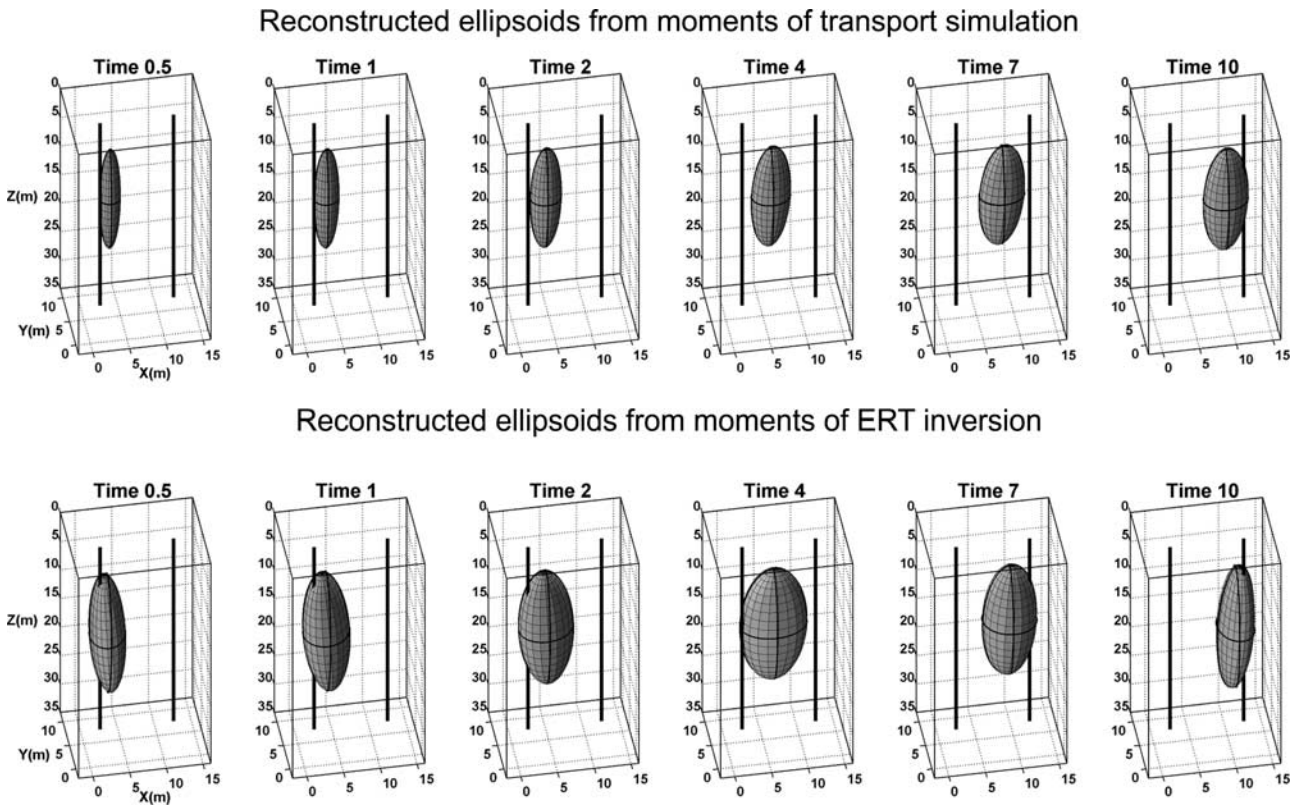

Figure 7. Reconstructed 3-D ellipsoids based on the full covariance matrix and center of mass as estimated from (top) transport simulations at multiple time steps and (bottom) the ERT inversions of those transport simulations. The horizontal and vertical axes of the ellipsoids are outlined in black. The injection and pumping wells are shown as thick lines. The ERT matches the proper center of mass. However, while the transport simulation shows continually increasing variance with time, the moments from the ERT show an increase and decrease in variance, likely associated with spatially variable resolution of the geophysical method.

gradient of 0.001. After the 9-hour tracer injection, freshwater injection was resumed for 20 days.

[38] The mass in the system at any time is calculated given the injection and pumping rates, the tracer concentrations at F626I and F626P, and an estimate of the NaCl concentration in the upgradient area. Because of the spatially variable NaCl concentration in the pore water as a function of the sewage plume on site the initial NaCl mass in the system is unknown. We therefore consider changes in mass through time net of the initial mass in the system as given by

$$M = \int Q_I C_I(t)dt + \int Q_B C_B(t)dt - \int Q_P C_P(t)dt \qquad (12)$$

where

M the total mass in the system net of initial mass, in mg;
Q_I injection well rate, in L/min;
Q_P pumping well rate, in L/min;
Q_B flow from the boundary that affects the tracer test, equal to Q_P -Q_I, in L/min;
C_I injection well concentration in mg/L;
C_P pumping well concentration in mg/L;
C_B concentration provided by the boundary, estimated to be 65 mg/L;
t time from start of tracer test.

The upgradient native groundwater concentration required to estimate C_B is poorly constrained by the upgradient well data. Fluid measurements taken from the multilevel sampler, wells neighboring the F626 array, and F626P prior to tracer injection suggest that a mean of 65 mg/L NaCl is appropriate. However, the range of NaCl concentration values varies from 22 to 74 mg/L depending on where the measurements were collected with respect to the sewage contaminated area. Although the measurements of NaCl concentration are spatially variable, cessation of the upgradient sewage dumping occurred approximately 10 years prior to the tracer test, so temporal changes in NaCl concentration at the boundaries are likely minimal over the timescale of this tracer test.

[39] Within the well cluster region all of the injected mass plus additional solute mass residing in the aquifer was pumped out. During the tracer test, we remove more mass than was initially injected because we also removed remnant pore fluid. The concentration history from F626P shows a broad peak with a maximum concentration on the 10th day after injection (Figure 8). Breakthrough occurred 5.5 days after injection. The maximum NaCl concentration at the pumping well is approximately 85 mg/L, only 1/25th of the initial concentration of the injected tracer, a consequence of dispersion and dilution. The concentration drops beneath the background level of 65 mg/L due to the injected

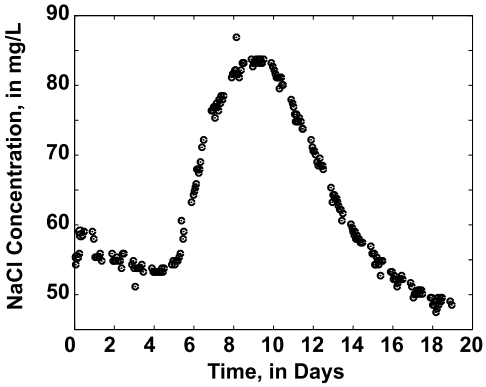

Figure 8. Sodium chloride concentration as measured at the pumping well versus time in days. Day zero corresponds to the start of the tracer test. The tracer was injected at F626I (Figure 2) beginning at time zero and continued for 9 hours. The elapsed time to peak arrival at the pumping well from the start of the injection period was 8.1 days.

freshwater chaser, and does not reach a steady value before the end of the data collection. Given the injection and pumping rates, the freshwater concentration, and an estimated background NaCl concentration of 65 mg/L, the NaCl concentration at the pumping well should plateau around 47 mg/L for this doublet test, compared to the 49 mg/L last measured from F626P.

[40] Before the start of the tracer test and prior to the injection of the freshwater tracer, a complete ERT data set was collected to provide the initial condition. Wells F626A, B, C, and D were each instrumented with 24 electrodes with 1-m separation, for a total of 96 electrodes. The electrodes used in the ERT survey were temporarily emplaced beneath the water table from 7.0 to 30.0 m below ground surface. Flexible well liners were inserted in the ERT wells after the electrode cables to prevent the well bore from acting as a hydraulic conduit; current injected between electrodes would preferentially travel in the well bore without this precaution. High contact resistance on site prevented the collection of surface resistivity data.

[41] Approximately 1000 resistance measurements were collected each hour using an IRIS R1 resistivity meter. Each complete 3-D ERT snapshot was collected over 6 hours and consisted of 3150 unique resistance measurements as well as 3150 reciprocal measurements [*Binley et al.*, 1995]. These resistance data were collected using a dipole-dipole configuration that combined current and potential dipoles that were in the same well and also split across two wells, as used in the synthetic ERT experiment. Source pairs were located in all 4 wells at multiple locations in depth. Given an average hydraulic conductivity of 100 m/d, effective porosity of 0.28, and an estimated pumping/injection hydraulic gradient of 0.0055, the tracer moved approximately 0.5 m during each 6-hour snapshot. Three 3-D data sets were collected each day for 20 days following the injection, for a total of 60 3-D data sets. In total, there were over 180,000 resistance measurements. Data with reciprocal errors larger than 5% were removed from the data sets prior to inversion.

[42] In addition to the tracer test, a pumping test and an infiltration experiment were conducted. The pumping test was conducted in F626P at pumping rate of 37.5 L/min, and the changes in head were measured at six neighboring wells within the array. Observed steady state occurred within 60 seconds given the highly permeable material and close proximity of the wells. The drawdown in F626P was approximately 1.8 cm, and the drawdown at the nearest well, F626C, was about 4.4 mm. Using the confined Theim equation [*Theim*, 1906] the estimated hydraulic conductivity was 102 m/d near F626P.

[43] The infiltration experiment was conducted during the tracer test using the water from the pumping well, which was diverted to a shallow excavation approximately 36 m from the nearest ERT well. Steady infiltration through a uniform incipient ponded area (less than 2 cm deep) was observed after 10 minutes, and the ponded area was observed to be stable for days. The measured infiltration area was approximately 1.1 m^2. Dividing the value discharged to the excavation, 37.5 L/min, by the infiltration area yields the infiltration rate. On the basis of saturated vertical flow under unity hydraulic gradient the vertical hydraulic conductivity is estimated to be $\sim$50 m/d.

6. Results of Field Experiment

6.1. Snapshot Tomograms Showing Tracer Migration

[44] Each resistance data set was inverted to create a tomogram that was subtracted from the preinjection regime tomogram. The sequence of these differenced tomograms shows changes in 3-D electrical conductivity (Figure 9). The tomograms clearly reflect the 3-D movement of the saline tracer through the aquifer over time. Inverting differenced data, rather than differencing post-inversion, is often preferred because systematic errors from the field and discretization errors in the forward modeling cancel [*Daily and Owen*, 1991; *LaBrecque and Yang*, 2000]. In this work, we found little difference between postprocessed tomograms and predifferenced tomograms. For each inversion, a rectangular prismatic finite element mesh with approximately 158,000 nodes and 149,100 elements was used. In the finite element mesh, resistivities are interpolated between nodes. Of the total elements considered in the inversion, only 26,000 elements are in the area of interest, which is $14 \times 10 \times 30$ m. The elements in this area are 0.5 m on a side. Although inversion of multiple 2-D image planes would be more computationally efficient, full 3-D ERT inversion is necessary to accurately estimate spatial moments because the electrical current is dependent on 3-D electrical conductivity structure.

[45] The ERT data set collected before the tracer test, prior to the freshwater injection, is difficult to use as a representative initial condition of a tracer-free aquifer for analyzing temporal changes in solute mass. The field site has spatially variable fluid electrical conductivity prior to tracer injection due to the presence of the remnant sewage plume. In addition, the introduction of freshwater into the aquifer, which had lower total dissolved solids than the in situ pore fluid, is clearly seen in the tomograms, although we cannot quantify the extent or mass of the freshwater from the tomograms alone. Consequently, the background (nontracer region) itself is time varying. As discussed presently, we estimate only the changes in tracer mass

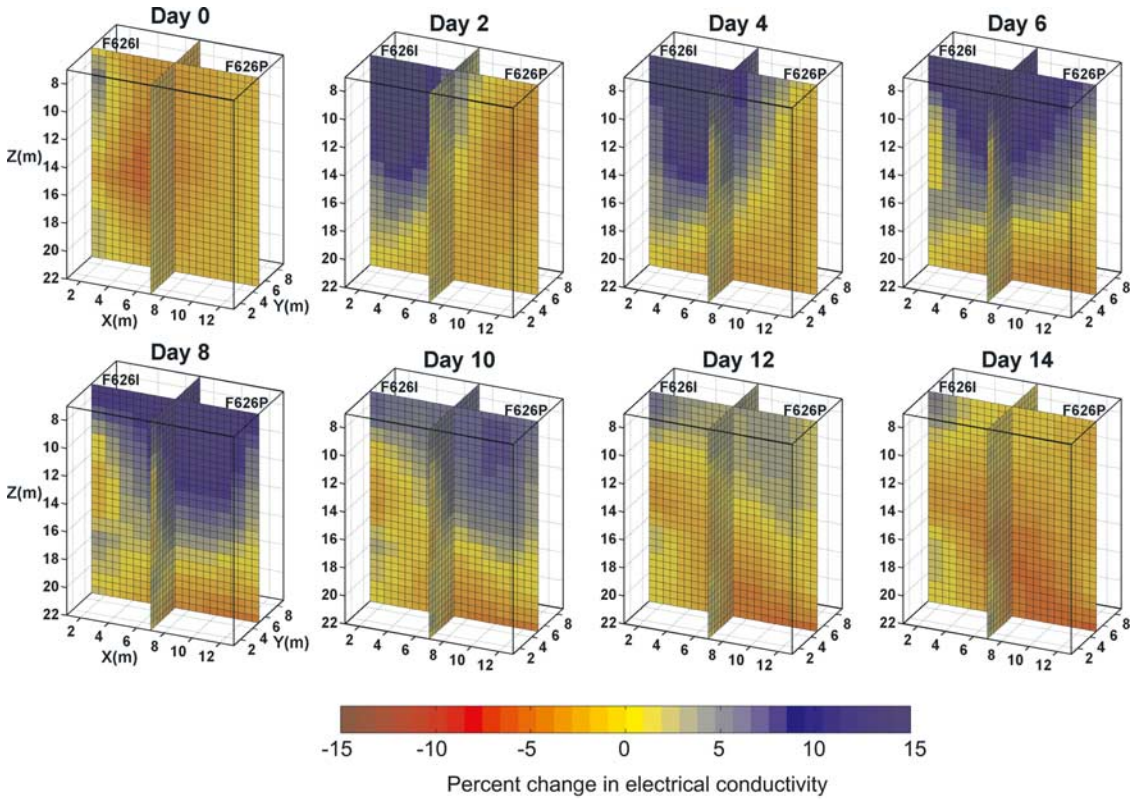

Figure 9. Snapshots of selected slices through 3-D tomograms indicating the percent change in electrical conductivity (EC) due to the injected sodium chloride tracer differenced from the initial EC conditions. Each data set is differenced from the initial condition collected prior to freshwater injection. Positive percent change in electrical conductivity (blue) indicates the presence of the tracer. Tracer migration from left to right is clearly seen. Red zones of increased electrical conductivity before and after the tracer fall below the background concentration due to resistive fresh water injection before and after the 9-hour tracer injection period.

through time by analyzing difference between subsequent snapshots.

6.2. Spatial Moments of Plumes Appearing in Tomograms

6.2.1. Zeroth Moment

[46] Using (8), changes in ERT-estimated mass in the system between snapshots were calculated. Changes between snapshots were inspected because the initial mass is unknown. We adopted the convention that preinjection baseline mass is assigned a value of zero, and positive values reflect mass added by tracer injection. Figure 10 displays a subset of images of temporal changes in mass based on zeroth moment analysis of the tomograms. These maps are plan view plots of the vertically summed change in mass calculated from the 3-D ERT inversions. Each change in mass plot is estimated from two sequential ERT inversions, separated in time by approximately 1 day. After day 11, there are no meaningful visible changes in electrical conductivity between days. Anomalous well bore effects do not entirely difference out, and are apparent at the four corner-point ERT wells in Figure 10 [*Osiensky et al.*, 2004].

[47] At early time, the tracer, shown in red as a positive change in mass, enters the system around F626I, on the left hand side of each image. Between days 3 and 5 after injection, the tracer plume is centrally located with respect to the electrodes, in an area of low sensitivity, and is therefore difficult to detect. The tracer is pumped from the aquifer between days 5.5 to 12 (Figure 8); the center of the tracer mass thus moves toward the pumping well and right-hand ERT well F6262C, and is increasingly better imaged. The injected freshwater also appears in the mass estimates as a negative change in mass (blue), which is correctly imaged both ahead of and behind the tracer itself. The freshwater tracer does not cancel out after differencing because it migrates over time in the induced flow field. After day 14, the tracer has been extracted at the pumping well and the changes in the images are minimal.

[48] The net ERT-estimated mass calculated from the changes shown in Figure 10 is compared to the actual tracer mass in the system estimated from injection and pumping well concentration histories (Figure 11). The ERT images display a slower increase in mass at early time and an extended plateau when compared to the mass based on measured concentration data. Also, the magnitude of mass is greatly underestimated. The relative ERT-estimated mass in Figure 11a shows a maximum injected mass of only 1.1 kg and a maximum-to-minimum mass change of approximately 5.2 kg, approximately 25% of the expected change in the NaCl mass in the system of 20.4 kg (15.3 kg injected and 5.1 kg of background mass). The ERT maps correctly show that more mass was removed from the aquifer than injected, mimicking the actual history of mass removal.

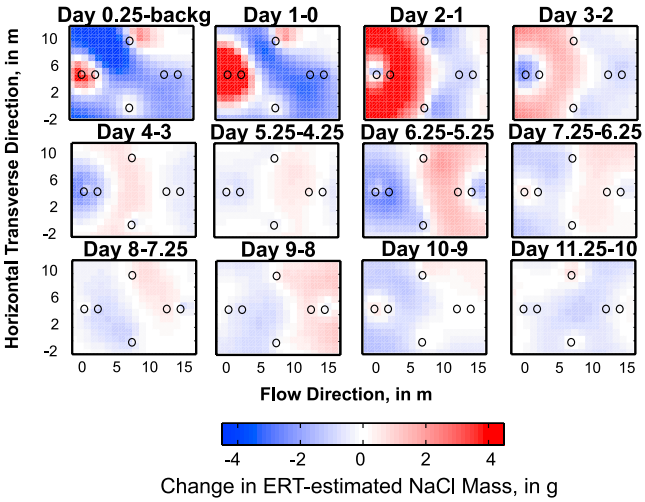

Figure 10. Map view of daily changes of depth-summed mass from ERT tomograms. Changes in mass are calculated using equation (8) and integrated horizontally. Red indicates areas of increased sodium chloride mass from previous day, and blue indicates decreased sodium chloride mass. The first time slice is differenced from the initial condition. Changes in mass over time reflect solute migration from left to right until day 9, when most of the tracer mass was removed by the pumping well. The ERT wells and pumping wells are shown as circles and correspond to those appearing in Figure 2. After day 11, few meaningful visible changes appear.

[49] At early time, the ERT greatly underestimates the mass in the system likely due to a combination of well bore artifacts and difficulty in inverting for small, concentrated objects. Between day 4 to day 10, the ERT consistently recovers approximately 10% of the true mass. At late time, after day 10, when the mass in the system is low and the ERT data become noisier with respect to the signal, ERT mass estimates are less reliable.

6.2.2. First Moment

[50] Estimates of the center of mass are based on snapshots differenced from the background. We subtract off the background from each snapshot despite the relative inaccuracies in the background image. The center of mass in the direction of flow estimated from images based on ERT shows a steady increase extending from the injection well at x = 2 m toward the pumping well at x = 12 m until day 9 after injection (Figure 12a). After day 9, the estimated center of mass in the direction of flow pulls back toward the injection well, due to the appearance upgradient of higher electrical conductivity artifacts. In the horizontal direction transverse to flow, the center of mass remains fairly consistent along the line where the center of mass should appear: y = 5 m (Figure 12b). In the vertical direction, the elevation of the center of mass is fairly consistent, following a line at a depth of 11 m, until day 11, at which point it appears to sink. This is likely an artifact due to low ERT sensitivity at later time as the tracer mass is removed from the system (Figure 12c).

6.2.3. Second Moment

[51] The spatial variance was determined by subtracting each snapshot from the background and then applying (8). In the direction of flow the variance is low at early and late times, and high between days 6 and 14 (Figure 13a). True spreading due to dispersion appears to be masked if not swamped by the affects of regularization. Once the tracer is centrally located, the spatial variance appears to increase due to the presence of well bore ERT artifacts. When the tracer is largely removed from the system, the spatial variance again decreases. The spatial variance in the direction transverse to flow remains approximately constant, which implies that the tracer, on average, remains equidistant between the ERT wells in the direction perpendicular to flow through time (Figure 13b). In the vertical direction, the variance remains constant until day 11, at which time it increases suddenly; again, likely an artifact of low sensitivity.

7. Comparison of Moments Estimated From Field and Synthetic ERT Experiments

[52] Tracer mass is underestimated, both in the synthetic experiment and the field data, given the overparameterized inverse problem. This result is not surprising, given that fewer data are collected than parameter values solved for; given realistic ERT data (quantity and quality), the inversion method requires some sort of assumed smoothing, zonation, correlation structure, or other regularization. The use of a smoothing constraint precludes the ability to accurately estimate mass, and the results presented here are applicable to other overparameterized ERT inversions. Collecting additional data in the field was not possible given temporal constraints on obtaining snapshot ERT-based images and the high contact resistance in the field that prevented the collection of surface resistivity data.

[53] Analyzing tracer mass, the mass recovery in the field is significantly worse than in the synthetic examples

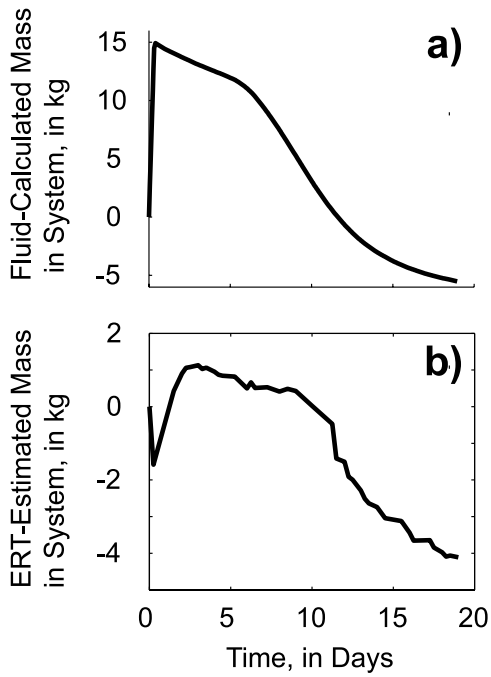

Figure 11. (a) Mass in system based on known mass injection and pumping histories. (b) Cumulative difference of ERT mass estimated from 3-D tomograms.

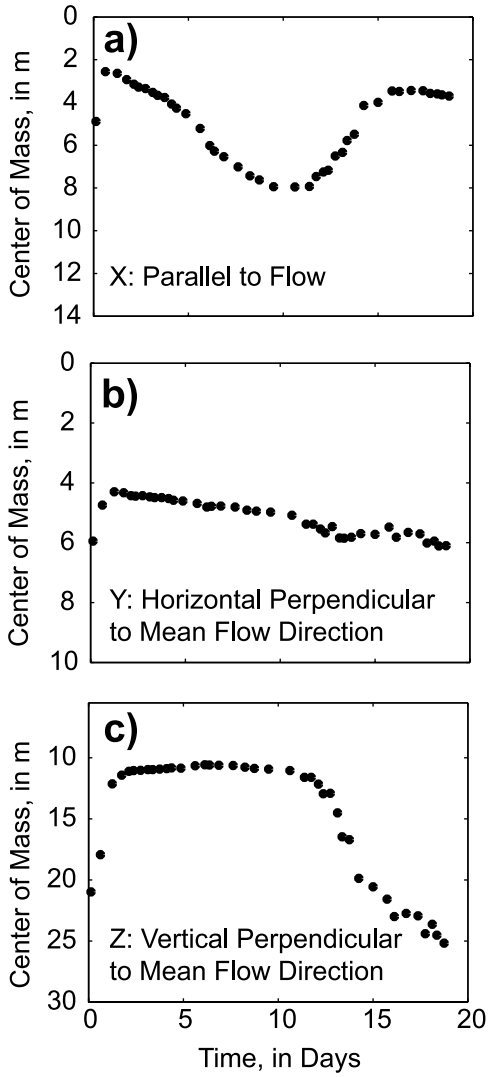

Figure 12. Center of mass calculated from analysis of the field ERT inversions in (a) direction of flow, (b) horizontal perpendicular to the mean flow, and (c) vertical perpendicular to the mean flow direction.

(Figures 4 and 11). This increased underestimation is likely due to subpixel heterogeneity, which is not considered in the synthetic models. Such field heterogeneity can define the chemical migration and possibly lead to small-scale preferential flow paths that may not be detected by the ERT. It is tough to estimate the scale of heterogeneity that would not be detected by the ERT as the spatial resolution of the method is difficult to quantify because it is controlled by electrode geometry, measurement schedule, and electrical conductivity distribution [*Daily and Ramirez*, 1995]. However, it is clear that we are not able to resolve targets (local conductivity values) smaller than the grid spacing, which is in this case 0.5 m on a side. Because of the low resolution of ERT, small targets like isolated fingers that may occur in the field are unlikely to be captured. Data noise may also explain the poor mass recovery of the field data when compared to the synthetic examples: nonstatic errors associated with electrical noise or instrumentation drift that often plague field data can be difficult to quantify. The choice of error misfit criteria will affect the resultant ERT mass estimates.

[54] Mass estimates from the ERT in both the field and synthetic examples show poor recovery at early time when the tracer plume is near the injection well. This result is likely due to the inability to recover high electrical conductivity contrasts. Also, both examples show poor moment estimates after day 11, when the tracer has largely been pumped from the aquifer and the remaining mass is dispersed such that the contrast between the tracer and background becomes small enough that the tracer is no longer a consequential target for the ERT. The percent differences between the field ERT data after day 11 and the background are no greater than 5%, which nearly falls within the noise: the ERT data from this field experiment have a reciprocal error of as much as 5%. Therefore the mass recovery is low in the field data. Also, unlike the synthetic examples, at late time the field data do not see a quick decrease in mass. The tail on the ERT-estimated mass in the field may be due to the presence of immobile mass [*Haggerty et al.*, 2004], which is not considered in the synthetic examples.

[55] In both the synthetic examples and the field experiment, the center of mass is accurately estimated using the ERT alone until approximately day 11. From these data, we could accurately estimate the average transport velocity and the average ratio of the hydraulic conductivity to porosity on site without the extensive drilling often required to estimate tracer center of mass information. However, estimation of the spatial variance from ERT, and consequently the dispersion coefficients, is often too high and does not accurately depict the true plume dispersion for these overparameterized inverse problems where a smoothing constraint is used to uniquely determine a solution. Consequently, ways of including additional data to reparameterize the inverse problem should be considered, although acquiring these data can be problematic in field settings where time and budget limitations may preclude extensive well drilling or additional data collection.

8. Conclusions

[56] In this work, we have demonstrated that transient ERT data can be used to estimate changes in tracer mass and center of mass through time in field settings. Three-dimensional time lapse ERT data were collected between four wells. The field experimental results provide basic and site-specific insights into the quantitative use of electrical geophysics to track tracer migration and quantify spatial moments over time. Despite complications in estimating the spatial moments, the geophysical data provide valuable new information regarding tracer location and mass that would be otherwise unobtainable given the scarcity of wells at this site.

[57] Simulation results suggest that calculated change in mass from the ERT inversions is only approximately 50% of the known change in mass from transport simulation, given the average flow behavior of the aquifer as well as the parameterization and regularization used to evaluate the ERT data. On the basis of simulation, ERT-estimated tracer mass is more significantly underestimated when the target volume is small and contrast is high, conditions for which

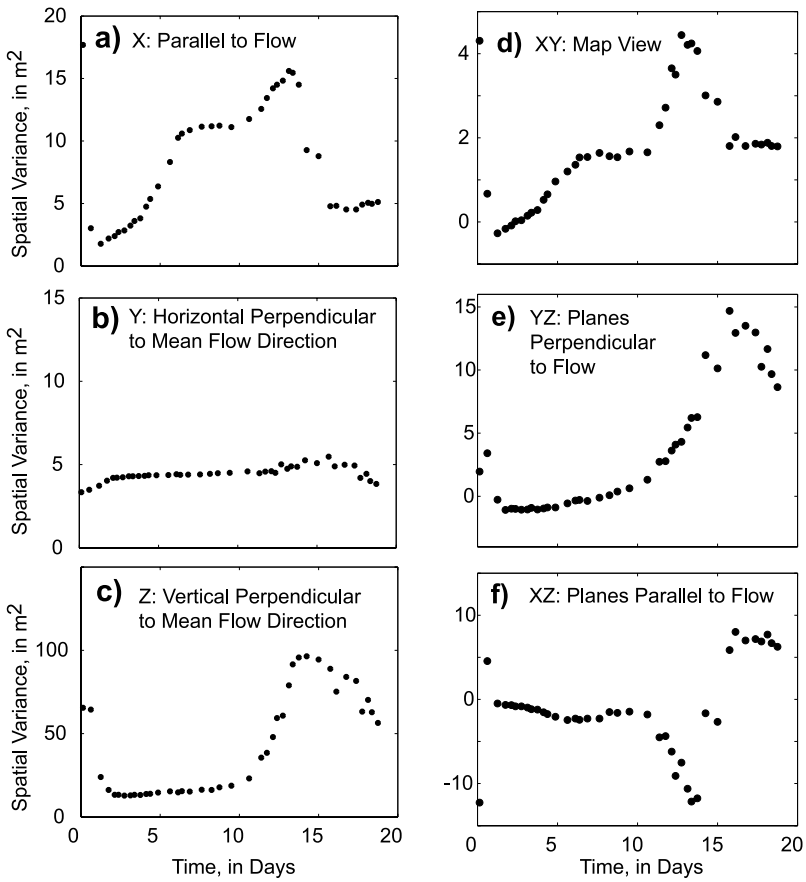

Figure 13. Spatial covariances calculated from analysis of the field ERT inversions in the (a) x direction, parallel to flow, (b) y direction, horizontal perpendicular to the mean flow, and (c) z direction, vertical perpendicular to the mean flow direction, and the (d) x-y cross covariance, map view, (e) y-z cross covariance, perpendicular to flow, and (f) x-z cross covariance, parallel to flow.

tomographic inversion has difficulty. In the field experiment, only 25% of the change in tracer mass is recovered in the inversions. The simple conversion of electrical conductivity to solute concentration based on Archie's law without consideration of spatially variable resolution drastically underestimated solute mass, due to spatially variable resolution and the choice of error misfit criteria used for inversion. However, in both the synthetic and field experiments, the timing of the breakthrough at the pumping well matches remarkably well with the ERT data and the center of mass is mapped well when the ERT is sensitive to the existence of the tracer.

[58] Low resolution, spatially variable target recovery, the choice of error criteria, and the effects of regularization from reconstruction complicate the use of ERT to quantitatively estimate the movement of a tracer in three dimensions. An understanding of these effects is important to using geophysical data quantitatively in estimating hydrogeologic properties of interest. The issues presented in this work plague the estimation of other hydrogeologic parameter values from overparameterized cross-well geophysical inversions, and must be considered when attempting to use these inversions to obtain more than a qualitative description of subsurface properties. Methods for reparameterizing the inverse problem should be considered to avoid the effects of overparameterization and smoothing from regularization that can impact the quantitative estimates of hydrogeologic parameter values using geophysical data.

[59] **Acknowledgments.** The authors wish to thank Andrew Binley of Lancaster University for use of his ERT inversion code, as well as numerous useful discussions. The advice and assistance of Denis LeBlanc, Kathy Hess, John W. Lane Jr., and Carole Johnson of the U. S. Geological Survey and the support of the USGS Toxic Substances Hydrology Program are gratefully acknowledged. We also thank Christopher Uyeda for his assistance in the field. We appreciate careful technical reviews by Fred Day-Lewis, Andreas Kemna, an anonymous reviewer, and the associate editor. This material is based upon work supported by the National Science Foundation under grant EAR-0124262. Any opinions, findings, and conclusions or recommendations expressed in this material are those of the authors and do not necessarily reflect the views of the National Science Foundation.

References

Acworth, R. I., and G. R. Dasey (2003), Mapping of the hyporheic zone around a tidal creek using a combination of borehole logging, borehole electrical tomography, and cross-creek electrical imaging, New South Wales, Australia, *Hydrogeol. J.*, *11*, 368–377.

Archie, G. E. (1942), The electrical resistivity log as an aid in determining some reservoir characteristics, *Trans. Am. Inst. Min. Metall. Pet. Eng.*, *146*, 54–62.

Archie, G. E. (1952), Classification of carbonate reservoir rocks and petrophysical considerations, *AAPG Bull.*, *36*, 278–298.

Aris, R. (1956), On the dispersion of a solute in a fluid flowing through a tube, *Proc. R. Soc. London, Ser. A*, *235*, 67–78.

Beck, J. V., B. Blackwell, and C. R. St. Clair Jr. (1985), *Inverse Heat Conduction: Ill-Posed Problems*, Wiley-Interscience, Hoboken, N. J.

Binley, A., A. Ramirez, and W. Daily (1995), Regularised image reconstruction of noisy electrical resistance tomography data, paper presented at 4th Workshop of the European Concerted Action on Process Tomography, Eur. Concerted Action on Process Tomography, Bergen, Norway.

Binley, A., S. Henry-Poulter, and B. Shaw (1996), Examination of solute transport in an undisturbed soil column using electrical resistance tomography, *Water Resour. Res.*, *32*(4), 763–769.

Binley, A., G. Cassiani, R. Middleton, and P. Winship (2002), Vadose zone flow model parameterisation using cross-borehole radar and resistivity imaging, *J. Hydrol.*, *267*, 147–159.

Boggs, J. M., S. C. Young, L. M. Beard, L. W. Gelhar, K. R. Rehfeldt, and E. E. Adams (1992), Field study of dispersion in a heterogeneous aquifer: 1. Overview and site description, *Water Resour. Res.*, *28*(12), 3281–3291.

Constable, S. C., R. L. Parker, and C. G. Constable (1987), Occam's inversion: A practical algorithm for generating smooth models from electromagnetic sounding data, *Geophysics*, *52*, 289–300.

Daily, W., and E. Owen (1991), Cross-borehole resistivity tomography, *Geophysics*, *56*, 1228–1235.

Daily, W., and A. Ramirez (1995), Electrical resistance tomography during in-situ trichloroethylene remediation at the Savannah River Site, *J. Appl. Geophys.*, *33*(4), 239–249.

Daily, W., A. Ramirez, D. LaBrecque, and J. Nitao (1992), Electrical resistivity tomography of vadose water movement, *Water Resour. Res.*, *28*(5), 1429–1442.

Day-Lewis, F. D., and J. W. Lane Jr. (2004), Assessing the resolution-dependent utility of tomograms for geostatistics, *Geophys. Res. Lett.*, *31*, L07503, doi:10.1029/2004GL019617.

Day-Lewis, F. D., J. W. Lane Jr., J. M. Harris, and S. M. Gorelick (2003), Time-lapse imaging of saline-tracer transport in fractured rock using difference-attenuation tomography, *Water Resour. Res.*, *39*(10), 1290, doi:10.1029/2002WR001722.

de Groot-Hedlin, C., and S. Constable (1990), Occam's inversion to generate smooth, two-dimensional models from magnetotelluric data, *Geophysics*, *55*, 1613–1624.

Freyberg, D. L. (1986), A natural gradient experiment on solute transport in a sand aquifer: 2. Spatial moments and the advection and dispersion of nonreactive tracers, *Water Resour. Res.*, *22*(13), 2031–2046.

Garabedian, S. P., and D. R. LeBlanc (1989), Overview of contaminant hydrology, geochemistry, and microbiology at the Cape Cod toxic waste research site, *U. S. Geol. Surv. Water Resour. Invest. Rep.*, *88-4220*, 133–142.

Garabedian, S. P., D. R. LeBlanc, L. W. Gelhar, and M. A. Celia (1991), Large-scale natural gradient tracer test in sand and gravel, Cape Cod, Massachusetts: 2. Analysis of spatial moments for a nonreactive tracer, *Water Resour. Res.*, *27*(5), 911–924.

Gouveia, W. P., and J. A. Scales (1997), Resolution of seismic waveform inversion: Bayes versus Occam, *Inverse Probl.*, *13*, 322–349.

Guyod, H. (1944), Fundamental data for the interpretation of electric logs, *Oil Wkly.*, *115*(38), 21–27.

Haggerty, R., C. F. Harvey, C. Freiherr von Schwerin, and L. C. Meigs (2004), What controls the apparent timescale of solute mass in aquifers and soils? A comparison of experimental results, *Water Resour. Res.*, *40*, W01510, doi:10.1029/2002WR001716.

Harbaugh, A. W., and M. G. McDonald (1996), User's documentation for MODFLOW-96, an update to the U.S. Geological Survey Modular finite-difference ground-water flow model, *U.S. Geol. Surv. Open File Rep.*, *96-485*.

Hess, K. M., S. H. Wolf, and M. A. Celia (1991), Estimation of macrodispersivities from the spatial variability of hydraulic conductivity in a sand and gravel aquifer, Cape Cod, Massachusetts, *U.S. Geol. Surv. Open File Rep.*, *91-4034*, 15–22.

Keller, G. V., and F. C. Frischknecht (1966), *Electrical Methods in Geophysical Prospecting*, Elsevier, New York.

Kemna, A., J. Vanderborght, B. Kulessa, and H. Vereeken (2002), Imaging and characterisation of subsurface solute transport using electrical resistivity tomography (ERT) and equivalent transport models, *J. Hydrol.*, *267*, 125–146.

Kitanidis, P. K. (1997), The minimum structure solution to the inverse problem, *Water Resour. Res.*, *33*(10), 2263–2272.

LaBrecque, D. J., and X. Yang (2000), Difference inversion of ERT data; a fast inversion method for 3-D in-situ monitoring, paper presented at Symposium on the Application of Geophysics to Engineering and Environmental Problems (SAGEEP), Environ. and Eng. Geophys. Soc., Arlington, Va.

LaBrecque, D. J., M. Miletto, W. Daily, A. Ramirez, and E. Owen (1996), The effects of noise on Occam's inversion of resistivity tomography data, *Geophysics*, *61*, 538–548.

Lane, J. W., Jr., F. D. Day-Lewis, R. J. Versteeg, and C. C. Casey (2004), Object-based inversion of crosswell radar tomography data to monitor vegetable oil injection experiments, *J. Environ. Eng. Geophys.*, *9*(2), 63–77.

LeBlanc, D. R. (1984), Sewage plume in a sand and gravel aquifer, Cape Cod, Massachusetts, *U.S. Geol. Surv. Water Supply Pap.*, *2218*.

LeBlanc, D. R., S. P. Garabedian, K. M. Hess, L. W. Gelhar, R. D. Quadri, K. G. Stollenwerk, and W. W. Wood (1991), Large-scale natural gradient tracer test in sand and gravel, Cape Cod, Massachusetts: 1. Experimental design and observed tracer movement, *Water Resour. Res.*, *27*(5), 895–910.

LeBlanc, D. R., K. M. Hess, D. B. Kent, R. L. Smith, L. B. Barber, K. G. Stollenwerk, and K. W. Campo (1999), Natural restoration of a sewage plume in a sand and gravel aquifer, Cape Cod, Massachusetts, *U.S. Geol. Surv. Water Resour. Invest. Rep.*, *99-4018C*, 245–259.

Liu, G., C. Zheng, and S. M. Gorelick (2004), Limits of applicability of the advection-dispersion model in aquifers containing connected high-conductivity channels, *Water Resour. Res.*, *40*, W08308, doi:10.1029/2003WR002735.

Mackay, D. M., D. L. Freyberg, P. V. Roberts, and J. A. Cherry (1986), A natural gradient experiment on solute transport in a sand aquifer: 1. Approach and overview of plume movement, *Water Resour. Res.*, *22*(13), 217–229.

Masterson, J. P., and P. M. Barlow (1994), Effects of simulated ground-water pumping and recharge on the ground-water flow in Cape Cod, Martha's Vineyard, and Nantucket Island Basins, Massachusetts, *U.S. Geol. Surv. Open File Rep.*, *94-316*.

Masterson, J. P., D. A. Walter, and J. Savoie (1997), Use of particle tracking to improve numerical model calibration and to analyze ground-water flow and contaminant migration, Massachusetts Military Reservation, western Cape Cod, Massachusetts, *U.S. Geol. Surv. Water Supply*, *2482*.

McLaughlin, D., and L. R. Townley (1996), A reassessment of the groundwater inverse problem, *Water Resour. Res.*, *32*(5), 1131–1161.

Oldale, R. N. (1969), Seismic investigations on Cape Cod, Martha's Vineyard, and Nantucket, Massachusetts, and a topographic map of the basement surface from Cape Cod Bay to the islands, *U.S. Geol. Surv. Prof. Pap.*, *650-B*.

Ory, J., and R. G. Pratt (1995), Are our parameter estimators biased? The significance of finite-difference regularization operators, *Inverse Probl.*, *11*, 397–424.

Osiensky, J. R., R. Nimmer, and A. Binley (2004), Borehole cylindrical noise during hole-surface and hole-hole resistivity measurements, *J. Hydrol.*, *289*, 78–94.

Park, S. K. (1998), Fluid migration in the vadose zone from 3-D inversion of resistivity monitoring data, *Geophysics*, *63*, 41–51.

Sasaki, Y. (1989), Two-dimensional joint inversion of magnetotelluric and dipole-dipole resistivity data, *Geophysics*, *54*, 254–262.

Singha, K., and S. Moysey (2004), Application of a new Monte Carlo approach to calibrating rock physics relationships: Examples using electrical resistivity and ground penetrating radar tomography, paper presented at Symposium on the Application of Geophysics to Engineering and Environmental Problems (SAGEEP), Environ. and Eng. Geophys. Soc., Colorado Springs, Colo.

Slater, L., A. M. Binley, W. Daily, and R. Johnson (2000), Cross-hole electrical imaging of a controlled saline tracer injection, *J. Appl. Geophys.*, *44*(2–3), 85–102.

Slater, L., A. Binley, R. Versteeg, G. Cassiani, R. Birken, and S. Sandberg (2002), A 3D ERT study of solute transport in a large experimental tank, *J. Appl. Geophys.*, *49*, 211–229.

Tarantola, A. (1987), *Inverse Problem Theory: Methods for Data Fitting and Model Parameter Estimation*, Elsevier, New York.

Theim, G. (1906), *Hydrologische Methoden*, Gebhardt, Leipzig, Germany.

Tiedeman, C. R., and P. A. Hsieh (2004), Evaluation of longitudinal dispersivity estimates from simulated forced- and natural-gradient tracer tests in heterogeneous aquifers, *Water Resour. Res.*, *40*, W01512, doi:10.1029/2003WR002401.

Tikhonov, A. N., and V. Y. Arsenin (1977), *Solutions of Ill-Posed Problems*, John Wiley, Hoboken, N. J.

Tripp, A. C., G. W. Hohmann, and C. M. Swift Jr. (1984), Two-dimensional resistivity inversion, *Geophysics*, *49*, 1708–1717.

Vasco, D. W., A. Datta-Gupta, and J. C. S. Long (1997), Resolution and uncertainty in hydrologic characterization, *Water Resour. Res.*, *33*(3), 379–397.

Winsauer, W. O., H. M. Shearin Jr., P. H. Masson, and M. Williams (1952), Resistivity of brine-saturated sands in relation to pore geometry, *AAPG Bull.*, *36*, 253–277.

Wyllie, M. R. J., and W. D. Rose (1950), Some theoretical considerations related to the quantitative evaluation of the physical characteristics of reservoir rock from electrical log data, *Trans. Am. Inst. Min. Metall. Pet. Eng.*, *189*, 105–118.

Yeh, T. C. J., and J. Simunek (2002), Stochastic fusion of information for characterizing and monitoring the vadose zone, *Vadose Zone J.*, *1*, 207–221.

Yeh, T. C. J., S. Liu, R. J. Glass, K. Baker, J. R. Brainard, D. L. Alumbaugh, and D. LaBrecque (2002), A geostatistically based inverse model for electrical resistivity surveys and its applications to vadose zone hydrology, *Water Resour. Res.*, *38*(12), 1278, doi:10.1029/2001WR001204.

Zheng, C. (1990), MT3D, a modular three-dimensional transport model for simulation of advection, dispersion, and chemical reactions of contaminants in groundwater system, Ada, OK, report, U.S. Environ. Prot. Agency, Washington, D. C.

Zheng, C., and P. P. Wang (1999), MT3DMS: A modular three-dimensional multispecies model for simulation of advection, dispersion and chemical reactions of contaminants in groundwater systems: Documentation and user's guide, contract report SERDP-99-1, U.S. Army Eng. Res. and Dev. Cent., Vicksburg, Miss.

S. M. Gorelick and K. Singha, Department of Geological and Environmental Sciences, Stanford University, Stanford, CA 94305-2115, USA. (ksingha@pangea.stanford.edu)